Diatomaceous earth incorporated floating magnetic beads for oil

by Mochamad Zakki Fahmi

Submission date: 10-Nov-2022 05:44PM (UTC+0800)
Submission ID: 1950067805
File name: tomaceous_earth_incorporated_floating_magnetic_beads_for_oil.pdf (1.75M)
Word count: 9004
Character count: 47927

Environmental Technology & Innovation 25 (2022) 102120

Contents lists available at ScienceDirect

Environmental Technology & Innovation

journal homepage: www.elsevier.com/locate/eti

Diatomaceous earth incorporated floating magnetic beads for oil removal on water

Satya Candra Wibawa Sakti [a,b,*], Nindayu Indrasari [a], Rizki Ainuna Wijaya [a,c], Mochamad Zakki Fahmi [a,b,*], Alfa Akustia Widati [a,b], Hwei Voon Lee [d], Takahiro Fujioka [c], Nuryono [e], Chun-Hu Chen [f]

[a] Department of Chemistry, Faculty of Science and Technology, Universitas Airlangga, Campus C, Mulyorejo, Surabaya 60115, Indonesia
[b] Supramodification Nano-Micro Engineering Research Group, Universitas Airlangga, Campus C, Mulyorejo, Surabaya 60115, Indonesia
[c] Graduate School of Engineering, Nagasaki University, 1-14 Bunkyo-machi, Nagasaki 852-8521, Japan
[d] Nanotechnology & Catalysis Research Centre (NANOCAT), Level 3, Block A, Institute for Advanced Studies, Universiti Malaya, 50603 Kuala Lumpur, Malaysia
[e] Department of Chemistry, Faculty of Mathematics and Natural Sciences, Universitas Gadjah Mada, Sekip Utara, Yogyakarta 55281, Indonesia
[f] Department of Chemistry, National Sun Yat-sen University, Kaohsiung 80424, Taiwan

ARTICLE INFO

Article history:
Received 22 September 2021
Received in revised form 10 November 2021
Accepted 11 November 2021
Available online 25 November 2021

Keywords:
Alginate
Diatomaceous earth
Magnetic separation
Oil spill
Buoyancy
Water purification

ABSTRACT

Water contamination by oil spills causes severe damage to the environment and human health. Oil adsorbents should be buoyant, effective oil-contact, and regenerable. In this study, diatomaceous-earth (DE)-incorporated magnetic alginate (Alg)-based beads, chemically modified to include phthalic or maleic anhydride (denoted as Alg/DE/Fe_3O_4-PA and Alg/DE/Fe_3O_4-MA), were developed. Internal cavities, formed by cavity-forming agents, made them buoyant. The beads were buoyant and magnetically responsive for 30 days. Maximum oil adsorption capacities of Alg/DE/Fe_3O_4-PA and Alg/DE/Fe_3O_4-MA were 29.7 and 21.0 times their weights, respectively. The pseudo-second order kinetics model ($R^2 \sim 0.999$, ARE ≤ 1.088, and $\chi^2 \leq 0.041$) and Freundlich isotherm model ($R^2 \sim 0.999$, ARE ≤ 0.1, and $\chi^2 \leq 3.37 \times 10^{-3}$) were used to determine these values. Both beads were magnetically regenerable for up to 20 cycles. DE pores improved oil adsorption capacity by facilitating intra-bead diffusion of surface adsorbed oil. This was confirmed by micro-structural characterization using surface micrographs, elemental distribution, porosity, thermal stability, crystalline phases, molecular vibrational behavior, and magnetic properties. Scanning electron microscopy and X-ray diffractometry analyses revealed spherical beads with well-distributed Fe_3O_4 spinel on the surfaces. The two adsorbent beads satisfied the criteria for oil-removal from water: buoyancy, high affinity towards various oil types, and magnetic re-collectability.

1. Introduction

Seawater contamination due to deliberate or accidental oil spills is a global concern. Growing fossil fuel demand has increased oil spill frequency during oil exploration, transportation, refining, and use. In the Deepwater Horizon oil spill

* Corresponding authors at: Department of Chemistry, Faculty of Science and Technology, Universitas Airlangga, Campus C, Mulyorejo, Surabaya 60115, Indonesia.
E-mail addresses: satya.sakti@fst.unair.ac.id (S.C.W. Sakti), m.zakki.fahmi@fst.unair.ac.id (M.Z. Fahmi).

https://doi.org/10.1016/j.eti.2021.102120

(the largest recorded oil spill in history) in the Gulf of Mexico (April 20–July 15, 2010), more than 3.19 million barrels of oil were accidentally released into the sea, covering the northern gulf coast by an oil layer (Beyer et al., 2016). Oil residues were detected in the five U.S. Gulf states of Texas, Louisiana, Mississippi, Alabama, and Florida (Thyng, 2019). A large film of low-biodegradable oil, which spreads rapidly over water, is formed during an oil spill. This floating layer is hazardous to marine biota and surrounding ecosystems (Campelo et al., 2021).

Numerous techniques have been developed for oil spill clean-up. Thermal, physical, chemical, and biological techniques, including in-situ burning, using boom-skimmers, dispersants and surfactants, have been used for bioremediation and oil adsorption (Abidli et al., 2020; Bullock et al., 2019; Hoang, 2018; Ke et al., 2021). In-situ burning is a large-scale method that removes oil from water surfaces by direct oil burning (Hoang, 2018). The combustion forms toxic gases, and residues that sink to the seabed, harming marine biota. Additionally, the spread of fire is difficult to control. The boom-skimmer method consists of two stages: localizing oil spills with booms and carrying oil into a reservoir using mechanical devices called skimmers (Wang et al., 2018). This method requires specific expensive tools. Bacterial consortiums can be used for oil bioremediation with limited efficiency. Not all bacterial species degrade oil, and those that do are substrate-specific (Mapelli et al., 2017). Simple and efficient methods for oil spill clean-up and oil separation are scarce. Oil removal from water surfaces using sorbents and sorbent-devices is eco-friendly and cost-effective (Hoang et al., 2021). Several low-cost adsorbents, such as biochar (Gurav et al., 2021), carbon (Yang et al., 2021), aluminosilicate clay (Akpomie et al., 2019), and cellulose-based materials (Chau et al., 2021; Hoang et al., 2018b), have been extensively investigated for oil adsorption. Oil-contaminated water clean-up adsorbents should have buoyancy, high affinity towards different oil types, and be recoverable for long-term applications.

Alginate (Alg) is naturally abundant and can be extracted from brown algae and seaweeds (Hambali et al., 2018; Nizami et al., 2020). It entraps water pollutants (heavy metal ions, basic dyes, and pharmaceuticals) due to its high content of acidic carboxylate groups (Nasrollahzadeh et al., 2021). However, recovery of contaminant-loaded Alg hydrogel from the medium is difficult, limiting its utility as an adsorbent. To overcome this limitation, magnetic iron-based particles of magnetite (Fe_3O_4) have been used (Ali et al., 2021). In this study, magnetic Alg was physically modified with diatomaceous earth (DE), followed by hollow bead-shaping in an ionic crosslinking solution to enhance buoyancy, porosity, surface area, and thermal stability. As reported in a previous publication, $NaHCO_3$ and $CaCO_3$ form internal cavities, endowed with magnetic beads, for buoyancy and stability. These properties facilitate oil removal from water surfaces (Sakti et al., 2021). DE filler was used for its physicochemical properties, such as particle size, surface area, porosity, thermal stability, and acid resistance. DE is an eco-friendly adsorbent (Sriram et al., 2020), sensor (Leonardo et al., 2016), catalyst (Đặng et al., 2021), and drug delivery system (Phogat et al., 2021). Although DE-based adsorbents effectively adsorb water pollutants, their sinkable behavior and difficult post-adsorption recovery make investigations challenging, and adsorption information scarce. There are no published reports on oil-contaminated water clean-up using DE-based floating adsorbents.

This study evaluated oil removal from water surfaces using floating DE-incorporated magnetic beads. Chemical modification of attaching acid anhydride groups, by adding phthalic anhydride (PA) and maleic anhydride (MA), was performed to enhance adsorption affinity of the beads towards various oil types, on the surface of various water types. Oil removal tests were performed by varying parameters such as initial pH, contact time, initial oil concentration, oil type, and water type, to evaluate oil clean-up feasibility of Alg/DE/Fe_3O_4-MA and Alg/DE/Fe_3O_4-PA. Kinetics, isotherms, recoverability, recyclability, floating stability, and magnetically driven properties were also studied. Physical and chemical properties of Alg/DE/Fe_3O_4-MA and Alg/DE/Fe_3O_4-PA that influence the clean-up performance were evaluated by various techniques. The magnetic, buoyant, and recyclable Alg/DE/Fe_3O_4-MA and Alg/DE/Fe_3O_4-PA beads facilitated effective, rapid, and eco-friendly oil-contaminated water clean-up.

2. Materials and methods

2.1. Materials

Analytical quality materials and chemicals were used in the experiment and used as received without any further purification, unless otherwise specified. DE and sodium alginate ($Na(C_6H_6O_6)_n$) were supplied by Wako (Japan). Magnetite (Fe_3O_4, >90%) was obtained from Kishida Chemical Co., Ltd. (Japan). Acetic acid (CH_3COOH, 98%), acetone (C_3H_6O, 99.5%), ammonium hydroxide (NH_4OH, 28%–30%), calcium carbonate ($CaCO_3$, 99.5%), hydrochloric acid (HCl, 37%), sodium bicarbonate ($NaHCO_3$, 99.8%), and sodium hydroxide (NaOH, 97%) were purchased from Sigma-Aldrich (Germany). Calcium chloride ($CaCl_2 \cdot 2H_2O$, 100%), ethanol (C_2H_5OH, 97%), hexane (C_6H_{14}, 99%), MA ($C_4H_2O_3$, 99%), and PA ($C_6H_4(CO)_2O$, 99%) were obtained from Merck (Germany). Artificial seawater powder (Marine Art-SF-1) was purchased from Osaka Yakken. Co., Ltd. (Japan). Castor oil, coconut oil, olive oil, and vegetable oil were purchased from a local market. Crude oil was obtained from oil drilling in Indonesia. Tap water was collected from our university.

2.2. Fabrication of buoyant DE/magnetic Alg composite bead

DE was activated through 3 M HCl solution contact for 2 h, 4000 rpm centrifugation for 15 min, repeated neutralization with demineralized water, and 100 °C oven drying for 12 h. Activated DE (0.25 g) was dispersed in 50 mL 1.5 wt% Alg solution and mixed at 750 rpm for 30 min. Fe_3O_4, $NaHCO_3$, and $CaCO_3$ (1:1:1) were dispersed in the mixture and stirred

for 30 min. The black viscous suspension obtained was dropped into 300 mL of 5 wt% $CaCl_2$ solution and stirred for complete gelation. Black beads formed were collected using a magnet, immersed in 300 mL of 6% CH_3COOH solution for 24 h, repeatedly neutralized with water, lyophilized, and labeled as Alg/DE/Fe_3O_4. Alg/Fe_3O_4 was prepared using a similar method, without DE addition.

2.3. Surface functionalization of the composite bead with acid anhydride

Alg/DE/Fe_3O_4 was stirred in acetone overnight before modification. It was refluxed with 0.05 mol L^{-1} PA in acetone at 55 °C for 3 h. After esterification, the black beads were magnetically recovered and washed with acetone, ethanol, and water. The lyophilized beads were labeled Alg/DE/Fe_3O_4-PA and used for characterization and adsorption tests. Alg/DE/Fe_3O_4-MA was prepared by a similar method, with MA used for modification instead of PA. Bead preparation and modification are shown in Fig. S1.

2.4. Characterization of as-prepared beads

Bead morphology was examined using a FlexSEM-1000 system (Hitachi, Japan) at 5 kV accelerating voltage. Freeze-dried beads were coated with a thin gold layer, using a sputtering system, to enhance electrical conductivity. Elemental composition was determined, and mapping was conducted, using an EDX system. Crystal structure was observed using X-Pert MPD (Philips, Germany) with 1.54443 Å Cu-K_α radiation, 5–90° diffraction angle, and 5 °C min^{-1} scan step. Thermal degradation was evaluated using a TGA 4000 system (Perkin Elmer, USA). Dried beads (15 mg) were placed inside a crucible and heated under pure N_2 atmosphere, from 30–800 °C, at a heating rate of 5 °C min^{-1}, and 20 mL min^{-1} N_2 flow rate. Magnetic properties were examined using a VSM-7400 series (Lake Shore, USA), by exposing dried beads (25 mg) to -8–8 kOe magnetic field range, at room temperature. The Brunauer–Emmett–Teller (BET) surface area, pore volume, and pore size distribution were analyzed using an accelerated surface area and porosimetry system (ASAP 2020, Micromeritics, USA). An IRTracer-100 spectrophotometer (Shimadzu, Japan) was used to investigate functional moieties on each bead. Powdered beads were mixed with KBr, and multiple scans were collected at 4 cm^{-1} resolutions, in the 4000–400 cm^{-1} wavenumber range. Alg/Fe_3O_4, Alg/DE/Fe_3O_4-MA, and Alg/DE/Fe_3O_4-PA bead sizes were measured using a digital caliper (Krisbow, Indonesia).

2.5. Oil removal and bead regeneration experiments

Coconut oil, vegetable oil, olive oil, and castor oil are widely used, and commonly found in domestic wastewater. Crude oil, an oil-drilling product, can be found in seawater around ports and oil-storage warehouses in Indonesia. Therefore, these oil removals were chosen as objects of research and analysis. Oil clean-up performance by Alg/Fe_3O_4, Alg/DE/Fe_3O_4-MA, and Alg/DE/Fe_3O_4-PA beads, at variable oil–water mixture pH, contact time, and initial oil concentration, have been published previously with a slight modification (Singh et al., 2017; Soares et al., 2017; Yaacob et al., 2018). The synthesized beads (0.015 g) were placed in contact with 15 mL of 66.67 g L^{-1} oil–water mixture, to investigate the influence of oil–water mixture pH on oil removal. Initial pH of the mixture was regulated using 0.1 mol L^{-1} HCl and 0.1 mol L^{-1} NaOH, and the mixture was equilibrated using an orbital shaker at 200 rpm for 2 h. Oil adsorbed by the beads at equilibrium (q_e, g of oil g of beads^{-1}) was calculated using Eq. (1) shown below (Hoang et al., 2018a):

$$q_e = \frac{m_{oil}}{m_0} = \frac{m_{total} - m_{water} - m_0}{m_0} \quad (1)$$

Here, m_{oil} and m_{water} are the masses (g) of adsorbed oil and water, respectively; m_{total} and m_0 are the bead masses (g) before and after adsorption, respectively. Similar protocols were used to examine adsorption kinetics and isotherms, by varying contact time in the range 5–120 min. Initial oil concentration was varied from 40 to 120 g L^{-1}. Experimental setup and tools for examining these variables are presented in Fig. 1.

Regeneration potential was investigated by equilibrating the beads with 15 mL of 100 g L^{-1} oil–water mixture at 200 rpm for 2 h. The beads were recovered magnetically, and repeatedly washed with n-hexane, methanol, water, and lyophilized before the next cycle. Twenty adsorption–desorption cycles were conducted to assess oil removal performance of the beads. Even though all adsorption experiments were carried out using the same method and under the same conditions, errors in the experiments could not be eliminated. Therefore, all oil adsorption measurements were performed in triplicate to maximize accuracy and reduce experimental errors.

3. Results and discussion

3.1. SEM analysis and EDX mapping

The micrographs show a significant difference between micro-surface and cross-section construction of the synthesized beads (Fig. 2). The surface micrograph showed spherical Alg/Fe_3O_4 beads with a coarse surface. Fe_3O_4 microaggregates were distributed all over the surface, confirming Fe_3O_4 attachment to the Alg matrix. Sieve-shaped DE disks were observed

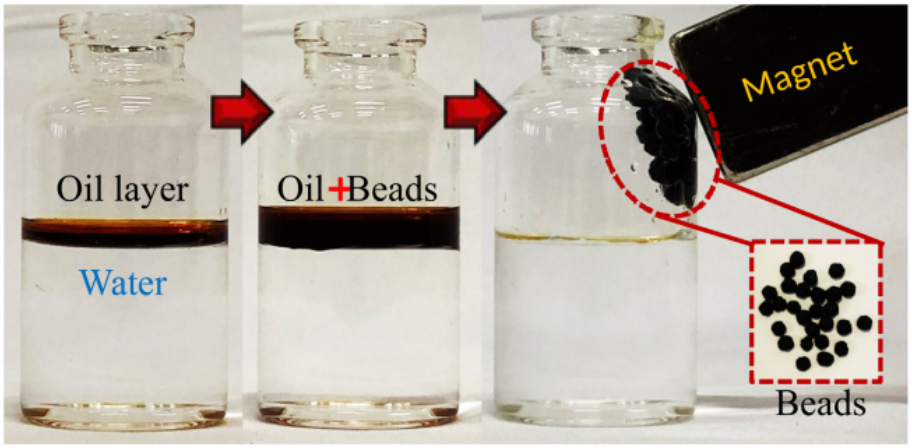

Fig. 1. Experimental setup of oil adsorption by as-synthesized beads.

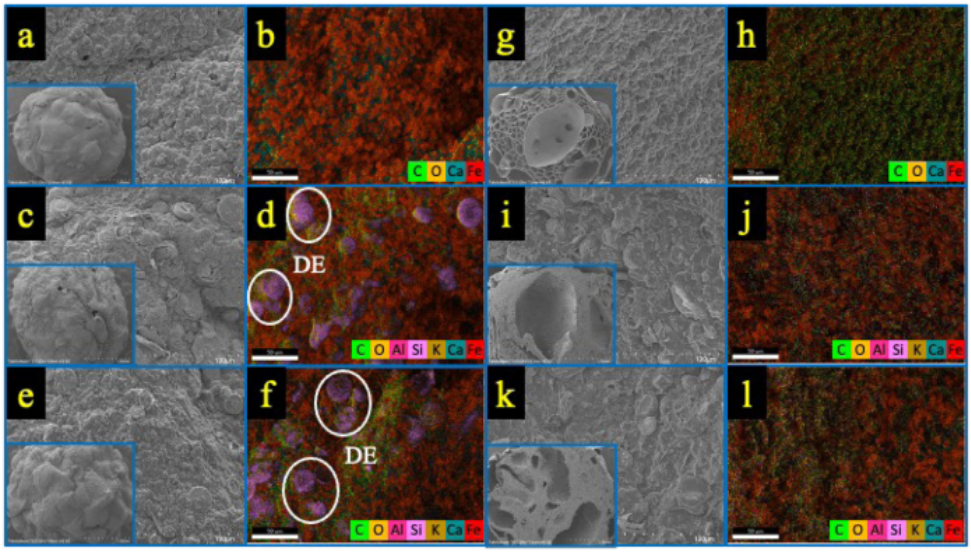

Fig. 2. Surface SEM micrograph (inset: whole bead micrograph) and EDX-mapping of (a,b) Alg/Fe_3O_4, (c,d) Alg/DE/Fe_3O_4-MA (e,f) Alg/DE/Fe_3O_4-PA and cross-section SEM micrograph (inset: whole bead micrograph) and EDX-mapping of (g,h) Alg/Fe_3O_4, (i,j) Alg/DE/Fe_3O_4-MA, and (k,l) Alg/DE/Fe_3O_4-PA.

on the Alg/DE/Fe_3O_4-MA and Alg/DE/Fe_3O_4-PA micro-surfaces, confirming homogeneous blending of DE. Compared to Alg/Fe_3O_4, Alg/DE/Fe_3O_4-MA and Alg/DE/Fe_3O_4-PA had rougher (with many wrinkles) surfaces with more pores, facilitating rapid intra-bead diffusion. An oval-shaped cavity was observed in the cross-sectional micrographs of Alg/Fe_3O_4, Alg/DE/Fe_3O_4-MA, and Alg/DE/Fe_3O_4-PA, due to the reaction of $NaHCO_3$ (as a porogen inside beads) with acetic acid. To maintain its spherical structure after $NaHCO_3$ dissolution by acetic acid, $CaCO_3$ was added as an internal crosslinking agent. Alg reacted with Ca^{2+}, a product of $CaCO_3$ dissolution, to form a rigid structure through ionotropic gelation.

Ca distribution on the outer and inner surfaces of the synthesized beads indicated complete ionotropic gelation. EDX mapping confirmed the presence of Fe on both outer and inner surfaces of Alg/Fe_3O_4, indicating successful entrapment of Fe_3O_4 in the Alg matrix (Fig. 2). DE presence in Alg/DE/Fe_3O_4-MA and Alg/DE/Fe_3O_4-PA was confirmed by observing Si (the major component of DE) distribution. CO_2 formation during $NaHCO_3$ and $CaCO_3$ dissolution forced inner DE to the outer surface, causing higher Si detection on the outer surface of Alg/DE/Fe_3O_4-MA and Alg/DE/Fe_3O_4-PA, than the inner surface. Alg/DE/Fe_3O_4-MA and Alg/DE/Fe_3O_4-PA surface contained 23%–27% Si, facilitating intra-bead diffusion. Small quantities (<5%) of DE minor components, Al and K, were also detected. Si, Al, and K were not detected on the Alg/Fe_3O_4 surfaces.

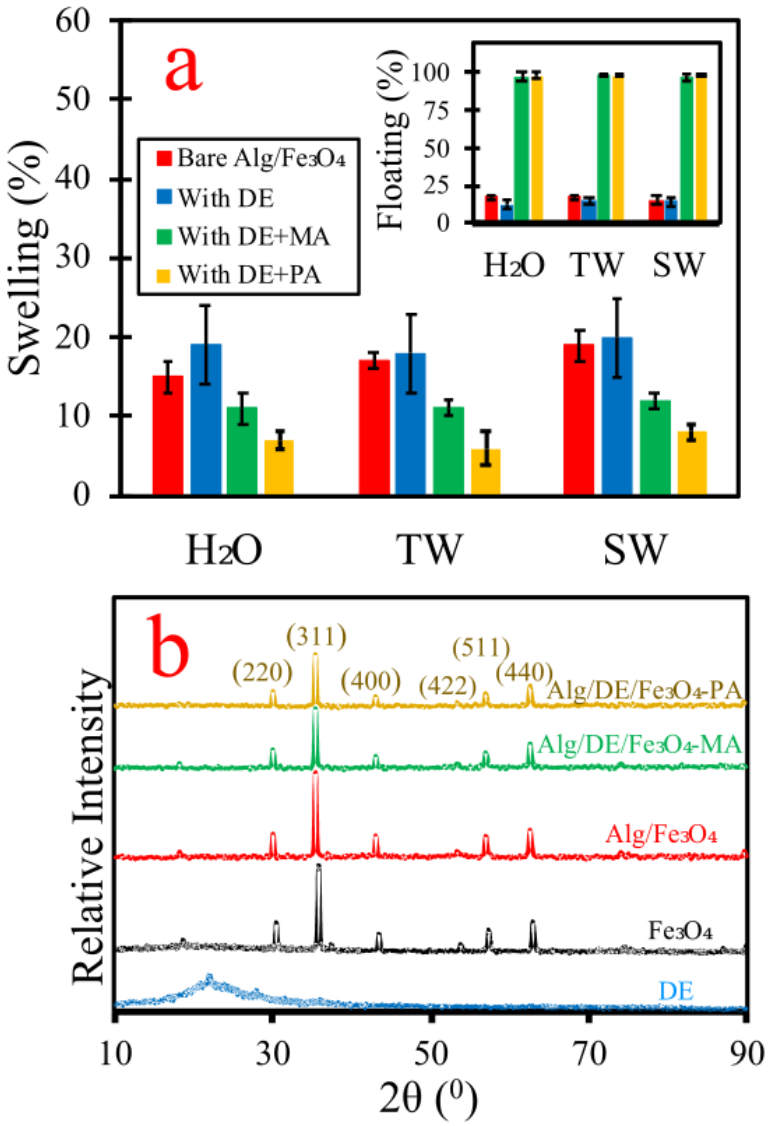

Fig. 3. (a) Swelling property (inset: self-floating property) in demineralized water, tap water and seawater and (b) XRD diffractogram of Alg/Fe_3O_4, Alg/DE/Fe_3O_4, Alg/DE/Fe_3O_4-MA and Alg/DE/Fe_3O_4-PA.

3.2. Physical dimensions, swelling, and buoyancy

Alg/DE/Fe_3O_4-PA and Alg/DE/Fe_3O_4-MA were observed to slightly increase in size, with unmodified shape, on DE entrapment and PA/MA attachment (Table 1). Penetration of water molecules into the gel bead-matrix through DE pores caused swelling. After MA/PA modification, bead surface hydrophilicity decreased, reducing water penetration into the gel matrix, decreasing the swelling ratio. Spherical shape enabled multi-directional oil diffusion into Alg/DE/Fe_3O_4-MA and Alg/DE/Fe_3O_4-PA, and both beads floated on demineralized water, tap water, and seawater, maintaining buoyancy for up to 30 days (Fig. 3(a)). Thus, high contact occurred between water-surface oils and Alg/DE/Fe_3O_4-MA, or Alg/DE/Fe_3O_4-PA.

3.3. XRD analysis

As shown in Fig. 3(b), sharp peaks observed in the Fe_3O_4 XRD pattern at 2θ values of 30.46°, 35.84°, 43.50°, 53.98°, 57.38°, and 62.92° corresponded to (220), (311), (400), (422), (511), and (440) plane reflections (Ghoochian et al., 2019; Sakthi Sri et al., 2020) of cubic Fe_3O_4 (JCPDS card No. 79-0418), respectively. For DE, amorphous and quartz phases of

Table 1
Physical dimension, textural and magnetic properties of Alg/Fe_3O_4, Alg/DE/Fe_3O_4-MA, and Alg/DE/Fe_3O_4-PA.

Magnetic bead	Component	Average bead size[a] (mm)	S_{BET}[b] (m g^{-1})	V_T[b] (cm^3 g^{-1})	D_P[b] (nm)	Hc[c] (G)	Ms[c] (emu g^{-1})	Mr[c] (emu g^{-1})	Mr/Ms
Alg/Fe_3O_4	Alginate, Fe_3O_4	2.81 ± 0.11	15.476	0.017	4.161	130.450	41.489	5.313	0.128
Alg/DE/Fe_3O_4-MA	Alginate, Fe_3O_4, Diatomaceous earth, Maleic anhydride	3.01 ± 0.21	24.740	0.038	4.931	118.440	29.008	3.484	0.120
Alg/DE/Fe_3O_4-PA	Alginate, Fe_3O_4, Diatomaceous earth, Phthalic anhydride	3.14 ± 0.19	35.058	0.045	5.832	120.440	23.094	2.850	0.123

[a]Average bead size was measured using a digital caliper (n = 100).
[b]S_{BET}, V_T and D_P were obtained from N_2 adsorption–desorption analysis.
[c]Hc, Ms, and Mr were measured using a vibrating sample magnetometer (VSM).

SiO_2 showed a broad peak centered at 22.14°, and a sharp peak at 28.20°. Crystalline quartz is commonly present in DE (Mota dos Santos and Cordeiro, 2021). After co-entrapment of Fe_3O_4 and DE in Alg/DE/Fe_3O_4-MA and Alg/DE/Fe_3O_4-PA, only peaks associated with Fe_3O_4 were detected in the diffractogram. This phenomenon is observed for Fe_3O_4 entrapment in other materials (Ewis et al., 2020; Li et al., 2020; Nuryono et al., 2016). This could be due to distribution of crystalline Fe_3O_4 on Alg/DE/Fe_3O_4-MA and Alg/DE/Fe_3O_4-PA surfaces, as confirmed by SEM analysis. Amount of entrapped Fe_3O_4 was confirmed to be higher in Alg/DE/Fe_3O_4-MA and Alg/DE/Fe_3O_4-PA, than DE, by EDX mapping.

3.4. Thermal stability

TGA and DTG curves of Fe_3O_4, Alg, Alg/Fe_3O_4, Alg/DE/Fe_3O_4, Alg/DE/Fe_3O_4-MA, and Alg/DE/Fe_3O_4-PA, are presented in Fig. 4(a–b). No decomposition was observed for Fe_3O_4 over the entire temperature range examined, because of its high thermal stability. In contrast, the thermograms of bare Alg beads and composite beads exhibited multistage degradation, with 205.65, 273.05, and 737.37 °C T_{max} values, respectively, corresponding to multi-step decomposition. Mass degradation at temperatures below 200 °C is associated with release of physically bound water molecules (Rigueto et al., 2021). In the first stage (below 200 °C), the bare Alg beads and Alg/Fe_3O_4 exhibited 9% and 7.78% mass losses, respectively, while Alg/DE/Fe_3O_4, Alg/DE/Fe_3O_4-MA, and Alg/DE/Fe_3O_4-PA lost less than 5% of their masses. In the second degradation stage (200–350 °C), caused by combustion of organic material, 38.32% bare Alg beads were degraded at T_{max} (273.05 °C) through polysaccharide ring splitting (Metin et al., 2020). In contrast, Alg/Fe_3O_4 and Alg/DE/Fe_3O_4 exhibited 14.52% and 12.24% mass losses, respectively, indicating suppression of decomposition, and enhancement of thermal stability on introduction of Fe_3O_4 and DE into the Alg matrix. Alg/DE/Fe_3O_4-MA and Alg/DE/Fe_3O_4-PA experienced 14% mass loss due to combustion of Alg matrix and MA/PA groups. In the final stage, 26.22% bare Alg bead mass was retained as an inorganic residue from the carbonization process (da Silva Fernandes et al., 2018), while the residual masses of Alg/Fe_3O_4, Alg/DE/Fe_3O_4, Alg/DE/Fe_3O_4-MA, and Alg/DE/Fe_3O_4-PA, were 66.24%, 72.71%, 64.86%, and 64.02%, respectively. This indicated improvement of Alg bead thermal stability by more than 2.4-fold on introduction of Fe_3O_4, DE, MA, and PA. By comparing their residual masses to that of Alg/DE/Fe_3O_4, the amount of MA and PA attached to the surface of Alg/DE/Fe_3O_4-MA and Alg/DE/Fe_3O_4-PA were found to be 7.85% and 8.69%, respectively.

3.5. Texture and pore distribution

As presented in Fig. S2(a–c), the N_2 adsorption/desorption isotherms were type IV, according to International Union of Pure and Applied Chemistry (IUPAC) classification, indicating mesoporous nature of Alg/Fe_3O_4, Alg/DE/Fe_3O_4-MA, and Alg/DE/Fe_3O_4-PA (Song et al., 2019). A mesoporous H4 type hysteresis loop could be observed in the isotherms at P/P^0 values of 0.21–0.86, 0.35–0.8, and 0.25–0.81 for Alg/Fe_3O_4, Alg/DE/Fe_3O_4-MA, and Alg/DE/Fe_3O_4-PA, respectively. Owing to DE on the surfaces, an H4 type hysteretic loop, associated with the presence of slit-like pores, was more evident in Alg/DE/Fe_3O_4-MA and Alg/DE/Fe_3O_4-PA, than in Alg/Fe_3O_4 (Song et al., 2021). Textural parameters and pore structures determined by N_2 adsorption/desorption experiments are listed in Table 1. Owing to higher porosity, Alg/DE/Fe_3O_4-MA and Alg/DE/Fe_3O_4-PA could generate more active sites for oil removal than Alg/Fe_3O_4.

3.6. Magnetic responsiveness of Alg/DE/Fe_3O_4-MA and Alg/DE/Fe_3O_4-PA

Magnetic responsiveness determined recovery of Alg/DE/Fe_3O_4-MA and Alg/DE/Fe_3O_4-PA from oil–water mixtures. As shown in Table 1 and Fig. S2(d), Ms value of Alg/Fe_3O_4 was lower than that of bare Fe_3O_4 (75.7 emu g^{-1}). DE entrapment and anchoring of magnetically non-responsive PA or MA, further reduced Ms values in Alg/DE/Fe_3O_4-PA and Alg/DE/Fe_3O_4-MA by 2.6-fold and 3.2-fold, respectively, compared to bare Fe_3O_4. Encapsulation effects, such as the presence of magnetically non-responsive Alg, DE, PA, and MA, caused this reduction. Similar phenomenon, on coating magnetic cores by different magnetically non-responsive matrices in similar materials, has been previously reported (Narita et al., 2019; Nuryono et al., 2020, 2014; Sakti et al., 2020, 2015; Armedya et al., 2019; Nuryono et al., 2014; Fahmi et al., 2020).

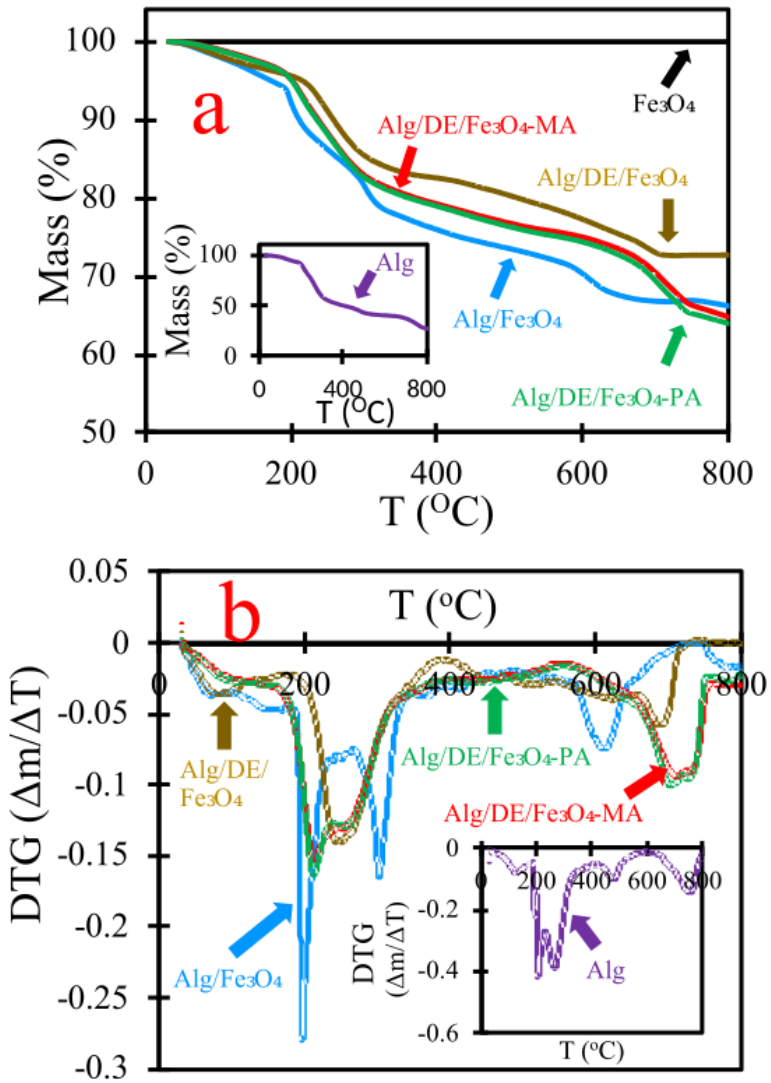

Fig. 4. (a) TGA thermogram (inset: thermogram of non-magnetic alginate) and (b) DTG thermogram (inset: thermogram of non-magnetic alginate) of Alg/Fe_3O_4, Alg/DE/Fe_3O_4, Alg/DE/Fe_3O_4-MA and Alg/DE/Fe_3O_4-PA.

3.7. Oil removal performance of Alg/DE/Fe_3O_4-MA and Alg/DE/Fe_3O_4-PA

3.7.1. Effect of Alg/DE/Fe_3O_4-MA and Alg/DE/Fe_3O_4-PA dosage and initial pH

As illustrated in Fig. 5(a), 0.25 g L^{-1} Alg/DE/Fe_3O_4-PA demonstrated higher adsorption capacity (19.2 g g^{-1}) than Alg/Fe_3O_4 and Alg/DE/Fe_3O_4-MA. At higher adsorbent dosage (1 g L^{-1}), it exhibited 1.5-fold increase in adsorption capacity, due to the presence of more vacant adsorption sites. However, increasing adsorbent dosage further (>1 g L^{-1}) caused insignificant change in oil adsorption due to reduction in contact area of oil with Alg/Fe_3O_4, Alg/DE/Fe_3O_4-MA, and Alg/DE/Fe_3O_4-PA, making fewer vacant sites and pores accessible.

Fig. 5(b) depicts oil adsorption efficiency as a function of pH, at optimum adsorbent to oil–water volume ratio. Oil adsorption changed negligibly with pH variation, indicating predominantly non-electrostatic forces in interfacial interactions of oil with Alg/Fe_3O_4, Alg/DE/Fe_3O_4-MA, and Alg/DE/Fe_3O_4-PA. At pH 6, considered to be the optimum pH, adsorption efficiency exhibited 9.5-fold increase in Alg/DE/Fe_3O_4-PA compared to Alg/Fe_3O_4. Phthalic benzene ring $\pi-\pi$ interactions in Alg/DE/Fe_3O_4-PA enhanced adsorption efficiency by amplifying non-electrostatic interactions. Oil adsorption was not conducted under highly basic conditions to avoid saponification of the oil layer by OH^-, and to prevent bead rupture and DE release by $Ca(OH)_2$, formed by reaction of Ca^{2+} (crosslinker) with excess OH^-.

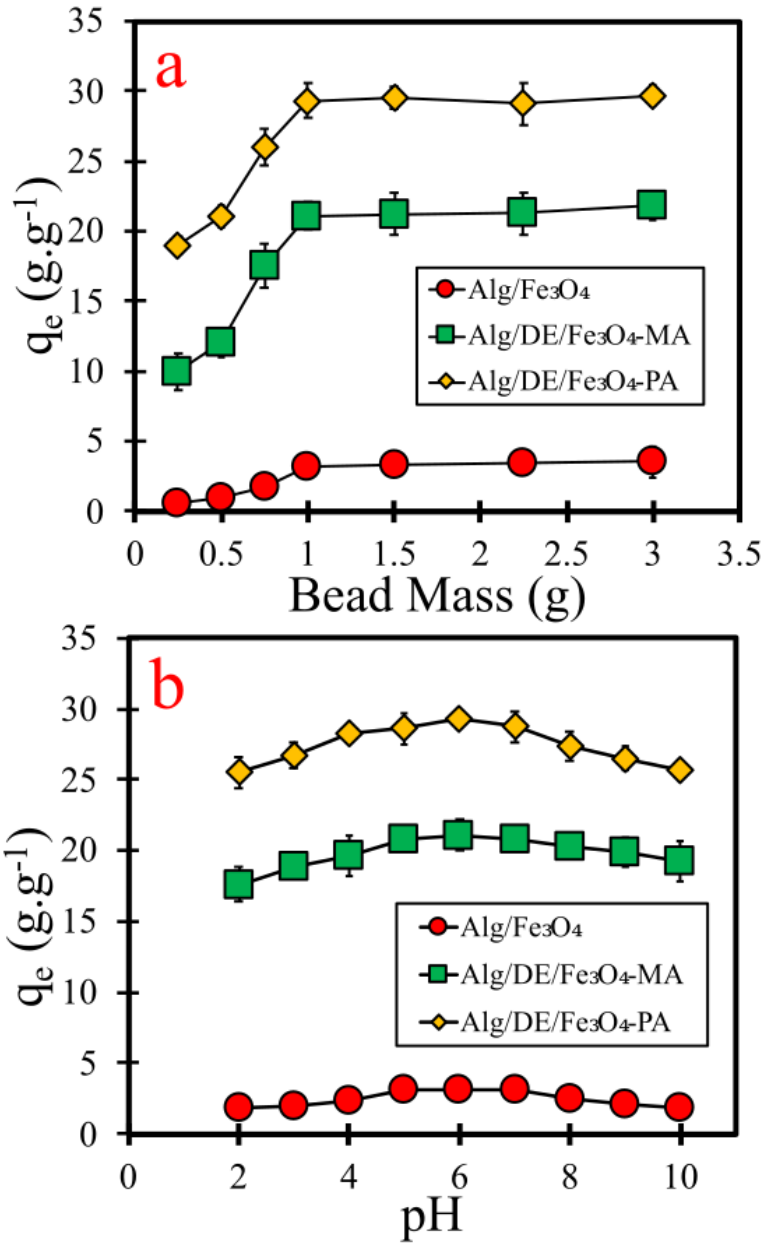

Fig. 5. Effect of (a) Alg/Fe_3O_4, Alg/DE/Fe_3O_4-MA and Alg/DE/Fe_3O_4-PA dosage (condition: C_0: 66.67 g L^{-1}, pH: 6, t: 2 h, T: 25 °C, and n: 3) and (b) initial pH on removal of crude oil (condition: C_0: 66.67 g L^{-1}, bead dose: 1 g L^{-1}, t: 2 h, T: 25 °C, and n: 3).

3.7.2. *Influence of contact time on oil removal*

Alg/DE/Fe_3O_4-MA and Alg/DE/Fe_3O_4-PA adsorbed oil up to 8.7 and 12 times their weights in the first 5 min, respectively, and oil adsorption increased exponentially with increasing contact time (Fig. 6(a)). This could be due to attachment of oil to the available active sites and pores of Alg/DE/Fe_3O_4-MA and Alg/DE/Fe_3O_4-PA. Gradually, most active sites and pores were occupied by oil, and equilibrium, indicated by a plateau region in the adsorption curve, was attained within 30 min. After equilibrium, oil adsorption by Alg/DE/Fe_3O_4-MA and Alg/DE/Fe_3O_4-PA became constant. The as-prepared beads attained oil-removal equilibrium within a short time, indicating their applicability in large-scale systems.

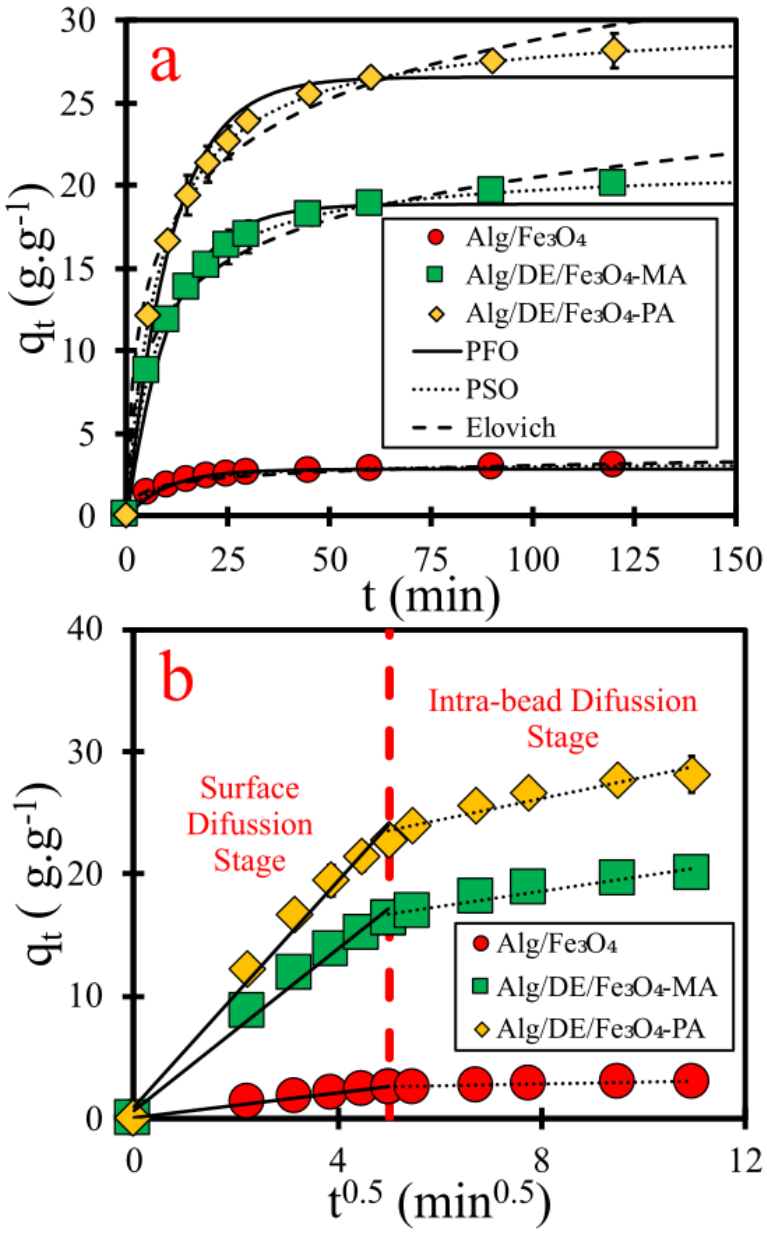

Fig. 6. (a) The non-linearized plot for PFO, PSO and Elovich kinetics model and (b) The linearized plot for IPD kinetics model (condition: C_0: 66.67 g L^{-1}, bead dose: 1 g L^{-1}, pH 6, T: 25 °C, and n: 3).

3.7.3. Evaluation of kinetics

Kinetics analysis (Fig. 6(a) and Table S1) revealed that oil removal by Alg/DE/Fe_3O_4-MA and Alg/DE/Fe_3O_4-PA did not follow the pseudo-first order and Elovich models, because both models produced low R^2 and high χ^2 and ARE values. The PSO model revealed a better fit to experimental data, with R^2 close to unity and lower χ^2 and ARE values. This indicated that oil removal by Alg/DE/Fe_3O_4-MA and Alg/DE/Fe_3O_4-PA could be analyzed by the PSO model. Alg/DE/Fe_3O_4-MA and Alg/DE/Fe_3O_4-PA were confirmed to be porous by SEM images and N_2 adsorption–desorption isotherms. Role of diffusion in their oil removal mechanism was assessed using the intraparticle diffusion (IPD) kinetics model. Fig. 6(b) shows that the IPD curve did not exhibit a single linear plot over time. It exhibited two segments, representing two different diffusion mechanisms. The first segment represented diffusion of oil to the external surface of Alg/DE/Fe_3O_4-MA and Alg/DE/Fe_3O_4-PA, passing through the boundary layer. This rapid surface-diffusion caused sharp increase in oil adsorption. Slow oil

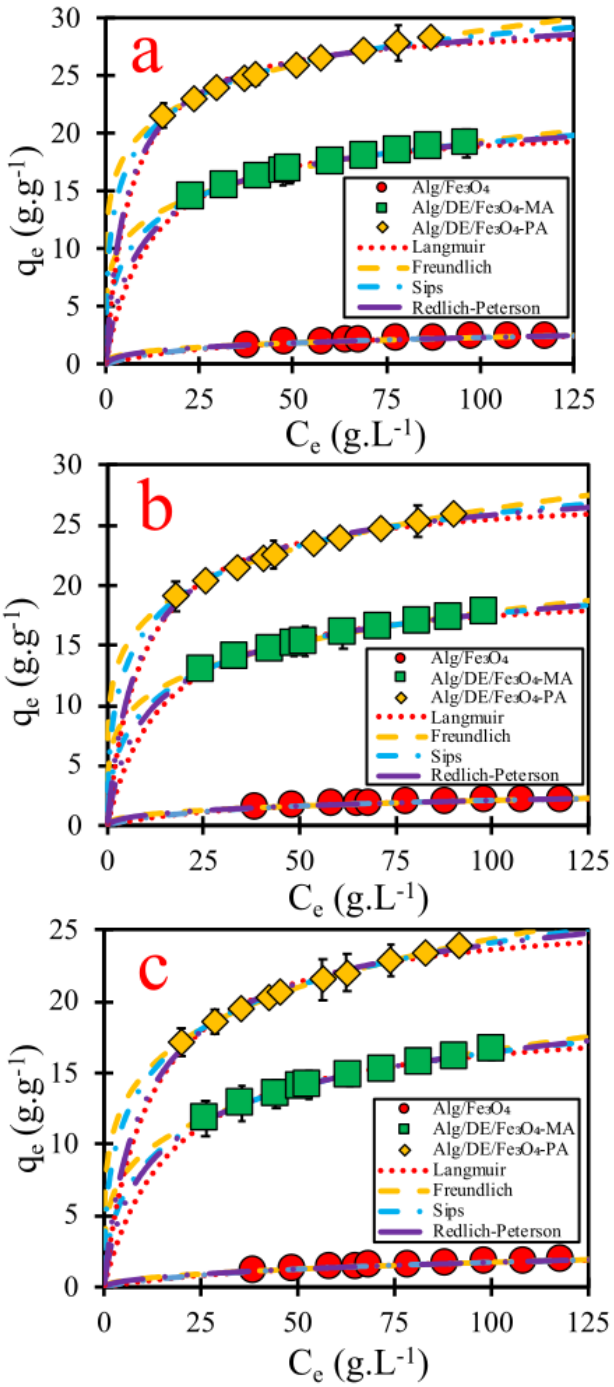

Fig. 7. Equilibrium Langmuir, Freundlich, Sips and Redlich–Peterson isotherms for removal of crude oil on deionized water surface by Alg/Fe_3O_4, Alg/DE/Fe_3O_4-MA and Alg/DE/Fe_3O_4-PA at (a) 25 °C, (b) 35 °C, and (c) 45 °C (condition: bead dose: 1 g L^{-1}, pH 6, t: 2 h, and n: 3).

adsorption, controlled by intra-bead diffusion, was represented by the second segment. In this segment, diffusion occurred inside DE pores, on Alg/DE/Fe_3O_4-MA and Alg/DE/Fe_3O_4-PA surfaces, resulting in lower value of $K_{2\text{-IPD}}$ than $K_{1\text{-IPD}}$. As presented in Table S1, the $K_{2\text{-IPD}}$ of Alg/DE/Fe_3O_4-PA was approximately 10 times higher than that of Alg/Fe_3O_4, due to

differences in surface morphology and pore profile, confirmed by SEM and N_2 adsorption–desorption analysis, respectively. Alg/Fe_3O_4 had a less porous surface, inhibiting rapid IPD of oil.

3.7.4. Influence of initial oil concentration

Significant increase in oil adsorption was observed at low initial oil concentration due to concentration gradient between the bulk oil–water mixture and Alg/DE/Fe_3O_4-MA, or Alg/DE/Fe_3O_4-PA surfaces (Fig. 7(a)). Increase of initial oil concentration intensified collisions between oil and Alg/DE/Fe_3O_4-MA or Alg/DE/Fe_3O_4-PA, leading to an increase in oil adsorption. At equilibrium, the active sites and pores of Alg/DE/Fe_3O_4-MA and Alg/DE/Fe_3O_4-PA were occupied, making oil adsorption constant. Alg/DE/Fe_3O_4-MA and Alg/DE/Fe_3O_4-PA showed 6.7-fold and 9.5-fold increase in Langmuir q_{max} in comparison to Alg/Fe_3O_4, respectively, indicating contribution of DE, MA, and PA to oil-molecule accommodation during adsorption.

3.7.5. Temperature dependence of isotherm models

Quality parameters from Langmuir, Freundlich, Sips, and Redlich–Peterson isotherm fittings were compared. The Freundlich parameter demonstrated a better fit for oil adsorption by Alg/DE/Fe_3O_4-MA and Alg/DE/Fe_3O_4-PA at 25 °C, with R^2 values close to unity, $\chi^2 \leq 3 \times 10^{-4}$, and ARE $\leq$ 0.0995 (Fig. 7(a–c) and Table S2.). Freundlich isotherm models revealed multilayer oil adsorption on Alg/DE/Fe_3O_4-MA and Alg/DE/Fe_3O_4-PA heterogeneous surfaces. The surfaces were heterogeneous due to DE pores and MA/PA attachment, as indicated by SEM images, N_2 adsorption–desorption profiles, and FTIR spectra. The homogeneous Alg/Fe_3O_4 surface adsorbed oil in the monolayer mode, as described by the Langmuir isotherm having R^2, χ^2, and ARE values of 0.9997, 6.94×10^{-5}, and 0.1375, respectively. The introduction of DE and MA/PA altered the synthesized adsorbent surface from homogeneous to heterogeneous, changing oil adsorption mechanism. Similar oil adsorption by Alg/DE/Fe_3O_4-MA and Alg/DE/Fe_3O_4-PA was observed at elevated temperatures (Table S2). Alg/DE/Fe_3O_4-MA and Alg/DE/Fe_3O_4-PA oil adsorption adhered to the Freundlich isotherm model at all studied temperatures (25–45 °C), while adsorption by Alg/Fe_3O_4 was best interpreted using the Langmuir model. The Langmuir q_{max} value of Alg/DE/Fe_3O_4-MA and Alg/DE/Fe_3O_4-PA decreased with temperature increase. This demonstrated influence of temperature on interfacial behavior of oil and the synthesized adsorbents. Decrease in oil viscosity on temperature elevation increased oil solubility and decreased Langmuir q_{max} values. Furthermore, non-electrostatic interaction between oil and Alg/DE/Fe_3O_4-MA or Alg/DE/Fe_3O_4-PA weakened with temperature increase, allowing easy oil detachment from the adsorbent pores and surfaces during post-adsorption recollection. Similar reduction in Langmuir q_{max} values with increasing temperature have been reported in previous publications (Mahmoud, 2020; Raj and Joy, 2015). Comparison of q_{max} values of Alg/DE/Fe_3O_4-MA and Alg/DE/Fe_3O_4-PA with Alg/Fe_3O_4, at all studied temperatures, confirmed that introduction of DE and MA/PA suppressed the reduction of Langmuir q_{max}.

3.8. Mechanism of oil removal

Oil removal mechanism was investigated by FTIR spectrophotometry of fresh and oil-loaded Alg/DE/Fe_3O_4-MA and Alg/DE/Fe_3O_4-PA, as shown in Fig. S3(a–d). In the FTIR spectrum of Fe_3O_4, several peaks were observed at 3665, 576, and 451 cm^{-1}, associated with O-H vibrations of adsorbed water, tetrahedral sites of Fe–O stretching, and octahedral sites of Fe-O stretching vibrations, respectively (Shahrashoub and Bakhtiari, 2021). After Fe_3O_4 incorporation, new peaks were observed at 1622 and 1419 cm^{-1}, corresponding to Alg C=O stretching (Lv et al., 2017). A weak peak at 1012 cm^{-1} was assigned to the Alg pyranose ring C–O group. DE presence in Alg/DE/Fe_3O_4-MA and Alg/DE/Fe_3O_4-PA was detected by peaks at 1091 and 802 cm^{-1}, associated with stretching vibration of siloxane (Si–O–Si) (Song et al., 2021, 2019). The attachment of MA and PA on the surface of Alg/DE/Fe_3O_4-MA and Alg/DE/Fe_3O_4-PA, respectively, was confirmed by a peak at 1720 cm^{-1}, assigned to MA/PA ester carbonyl group asymmetric stretching. A peak at 1595 cm^{-1} was attributed to C=C in MA/PA. A peak at 2850 cm^{-1}, assigned to C-H stretching vibrations, indicated ester bond formation (Yadav et al., 2019).

Crude oil, castor oil, coconut oil, vegetable oil, and olive oil consist mainly of hydrocarbons; therefore, related peaks were observed in the FTIR spectra. Peaks at 2910 and 2850 cm^{-1}, associated with C–H asymmetric and $-CH_2-$ symmetric stretching vibrations, respectively, were observed in all the oil spectra (Neves and Poppi, 2020). A peak at 1745 cm^{-1}, attributed to C=O stretching vibration of the fatty acid ester group, was observed in the FTIR spectra of edible oils, such as castor oil, coconut oil, vegetable oil, and olive oil (Jamwal et al., 2021). This peak was absent in the FTIR spectrum of crude oil (mainly composed of aliphatic and aromatic structures of carbon and hydrogen). A peak at 1456 cm^{-1} was assigned to C–H bending of $-CH_2-$ or $-CH_3$ (Tarhan, 2020). After oil adsorption, the above-mentioned peaks were observed in the FTIR spectra of oil-loaded Alg/DE/Fe_3O_4-MA and Alg/DE/Fe_3O_4-PA, indicating adsorbed oil molecules. A slight shift to lower wavenumbers could be observed for C=O and C-H vibrations of edible oils after adsorption, indicating physical attachment of the oil (Ewis et al., 2020). Interactions ($\pi-\pi$) facilitated by DE pores, between oil and MA/PA moieties of Alg/DE/Fe_3O_4-MA and Alg/DE/Fe_3O_4-PA, could be responsible for this attachment.

3.9. Practical feasibility analysis

Oil spills can occur in various aquatic environments. The components of simulated seawater are listed in Table S3. To evaluate applicability of Alg/DE/Fe_3O_4-MA and Alg/DE/Fe_3O_4-PA in oil-contaminated water clean-up, various water types were used as adsorption test media. Alg/DE/Fe_3O_4-MA and Alg/DE/Fe_3O_4-PA exhibited similar oil adsorption, regardless of water type used. Oil adsorption was slightly higher from seawater than demineralized or tap water. Screening effect could be responsible for this phenomenon. High concentration of counter ions in seawater, such as Na^+, Mg^{2+}, and Ca^{2+} can cause Alg matrix-surface neutralization, diminishing adsorbent-oil electrostatic repulsion. Furthermore, oil solubility in high-salinity seawater is low, leading to many effective collisions of oil with Alg/DE/Fe_3O_4-MA and Alg/DE/Fe_3O_4-PA, enhancing oil adsorption (Diraki et al., 2019).

Oil adsorption by Alg/DE/Fe_3O_4-MA and Alg/DE/Fe_3O_4-PA increased in the following order: crude oil < olive oil < vegetable oil < coconut oil < castor oil. This could be explained by oil density. Liquid pollutants such as high-density oils can easily accumulate in adsorbents. Thus, the adsorption of high-density oil was relatively higher than that of low-density oil. The relationship between oil density and adsorption for Alg/DE/Fe_3O_4-MA and Alg/DE/Fe_3O_4-PA is illustrated in Fig. S4(a). Differences in adsorption capacities of Alg/DE/Fe_3O_4-MA and Alg/DE/Fe_3O_4-PA towards various oil types were negligible, indicating their wide applicability.

Fig. S4(b–d) shows the reusability of Alg/DE/Fe_3O_4-MA and Alg/DE/Fe_3O_4-PA for removal of various oil types from different aqueous media. Reusability of the as-synthesized adsorbents, obtained by comparing oil adsorption before and after 20 adsorption cycles, decreased in the following order: Alg/DE/Fe_3O_4-PA > Alg/DE/Fe_3O_4-MA > Alg/Fe_3O_4. After 20 adsorption cycles, Alg/DE/Fe_3O_4-PA exhibited up to 95% adsorption capacity, regardless of oil or water type, while Alg/Fe_3O_4 lost more than 15% of its adsorption capacity. Thus, DE, MA, or PA introduction improved reusability and adsorption capacity of the synthesized beads. As presented in Table S4, Alg/DE/Fe_3O_4-MA and Alg/DE/Fe_3O_4-PA exhibited higher adsorption than previously reported magnetic adsorbents. Several reported Fe_3O_4-based adsorbents have higher M_s and shorter t_{eq} values due to their small sizes. However, small size enables facile oxidation of Fe_3O_4 to Fe_2O_3 after several adsorption–desorption cycles, especially in high-salinity seawater, weakening magnetic properties, making post-adsorption recovery difficult, and causing secondary pollution. The Alg matrix in Alg/DE/Fe_3O_4-MA and Alg/DE/Fe_3O_4-PA protected Fe_3O_4 from oxidation. Both Alg/DE/Fe_3O_4-MA and Alg/DE/Fe_3O_4-PA maintained their buoyancy over several oil adsorption–desorption cycles. Therefore, the as-synthesized Alg/DE/Fe_3O_4-MA and Alg/DE/Fe_3O_4-PA beads meet the criteria for effective and eco-friendly oil removal from aquatic environments.

4. Conclusions

This study reports the synthesis of magnetically driven Alg/DE composite beads, modified with PA/MA, for oil-contaminated water clean-up. High buoyancy of beads allowed intensive contact with aqueous oil films, removing oil within 30 min, following the PSO model (R^2 ~0.999, $\chi^2 \leq 0.041$, and ARE ≤ 1.088). Owing to the presence of DE molecules and PA/MA groups, the modified magnetic beads exhibited high adsorption capacity towards different oils, with maximum adsorption capacity values up to 29.7 times their weights, described by the Freundlich model, with R^2 ~0.999, $\chi^2 \leq 3.37 \times 10^{-3}$, and ARE ≤ 0.1. Oil adsorption was pH independent and extremely effective in deionized water, tap water, and seawater. Owing to high Ms values, confirmed by VSM data, the as-prepared beads were magnetically recoverable and regenerable over 20 oil adsorption–desorption cycles. Unique features of the magnetically driven PA/MA-modified Alg/DE composite beads demonstrated their potential as efficient and eco-friendly adsorbents for oil-contaminated water clean-up. Future research could include real-time analysis of the as-synthesized beads in environmental applications, evaluating their environmental effects, and biodegradability. Combination of the composite beads with other techniques, such as floating booms or oil-degrading mechanisms, could also be investigated for cost-effective solutions to mitigate the adverse effects of a large-scale oil spill.

CRediT authorship contribution statement

Satya Candra Wibawa Sakti: Conceptualization, Methodology, Investigation, Writing – original Draft. **Nindayu Indrasari:** Investigation. **Rizki Ainuna Wijaya:** Investigation. **Mochamad Zakki Fahmi:** Investigation, Funding acquisition. **Alfa Akustia Widati:** Investigation, Funding acquisition. **Hwei Voon Lee:** Investigation. **Takahiro Fujioka:** Writing – review & editing. **Nuryono:** Conceptualization. **Chun-Hu Chen:** Writing – review & editing, Funding acquisition.

Declaration of competing interest

The authors declare that they have no known competing financial interests or personal relationships that could have appeared to influence the work reported in this paper.

Acknowledgments

The authors would like to acknowledge the Ministry of Research, Technology, and Higher Education of the Republic of Indonesia for supporting this research project through the PDUPT Project under contract No. 809/UN3.14/PT/2020. This manuscript is dedicated to the memory of our dear friend and esteemed research group member, Dr. Abdulloh.

Appendix A. Supplementary data

Supplementary material related to this article can be found online at https://doi.org/10.1016/j.eti.2021.102120.

References

Abidli, A., Huang, Y., Cherukupally, P., Bilton, A.M., Park, C.B., 2020. Novel separator skimmer for oil spill cleanup and oily wastewater treatment: From conceptual system design to the first pilot-scale prototype development. Environ. Technol. Innov. 18, 100598. http://dx.doi.org/10.1016/j.eti.2019.100598.

Akpomie, K.G., Onyeabor, C.F., Ezeofor, C.C., Ani, J.U., Eze, S.I., 2019. Natural aluminosilicate clay obtained from south-eastern Nigeria as potential sorbent for oil spill remediation. J. Afr. Earth Sci. 155, 118–123. http://dx.doi.org/10.1016/j.jafrearsci.2019.04.013.

Ali, N., Hassan Riead, M.M., Bilal, M., Yang, Y., Khan, A., Ali, F., Karim, S., Zhou, C., Wenjie, Y., Sher, F., Iqbal, H.M.N., 2021. Adsorptive remediation of environmental pollutants using magnetic hybrid materials as platform adsorbents. Chemosphere 284, 131279. http://dx.doi.org/10.1016/j.chemosphere.2021.131279.

Armedya, Tri Prasetyo, Dzikri, Muhammad Fathan, Sakti, Satya Candra Wibawa, Abdulloh, Abdulloh, Raharjo, Yanuardi, Wafiroh, Siti Wafiroh, Purwati, Purwati, Fahmi, Mochamad Zakki, 2019. Kinetical release study of copper ferrite nanoparticle incorporated on PCL/collagen nanofiber for naproxen delivery. BioNanoScience 9, 274–284. http://dx.doi.org/10.1007/s12668-019-00618-y.

Beyer, J., Trannum, H.C., Bakke, T., Hodson, P.V., Collier, T.K., 2016. Environmental effects of the Deepwater Horizon oil spill : A review. MPB 110, 28–51. http://dx.doi.org/10.1016/j.marpolbul.2016.06.027.

Bullock, R.J., Perkins, R.A., Aggarwal, S., 2019. In-situ burning with chemical herders for Arctic oil spill response: Meta-analysis and review. Sci. Total Environ. 675, 705–716. http://dx.doi.org/10.1016/j.scitotenv.2019.04.127.

Campelo, R.P. de S., Lima, C.D.M. de, de Santana, C.S., Jonathan da Silva, A., Neumann-Leitão, S., Ferreira, B.P., Soares, M. de O., Melo Júnior, M. de, Melo, P.A.M. de C., 2021. Oil spills: The invisible impact on the base of tropical marine food webs. Mar. Pollut. Bull. 167, http://dx.doi.org/10.1016/j.marpolbul.2021.112281.

Chau, M.Q., Truong, T.T., Hoang, A.T., Le, T.H., 2021. Oil spill cleanup by raw cellulose-based absorbents: a green and sustainable approach. Energy Sources A 00, 1–14. http://dx.doi.org/10.1080/15567036.2021.1928798.

da Silva Fernandes, R., de Moura, M.R., Glenn, G.M., Aouada, F.A., 2018. Thermal, microstructural, and spectroscopic analysis of Ca^{2+} alginate/clay nanocomposite hydrogel beads. J. Mol. Liq. 265, 327–336. http://dx.doi.org/10.1016/j.molliq.2018.06.005.

Đặng, T.H., Nguyễn, X.H., Chou, C.L., Chen, B.H., 2021. Preparation of cancrinite-type zeolite from diatomaceous earth as transesterification catalysts for biodiesel production. Renew. Energy 174, 347–358. http://dx.doi.org/10.1016/j.renene.2021.04.068.

Diraki, A., Mackey, H.R., Mckay, G., Abdala, A., 2019. Removal of emulsified and dissolved diesel oil from high salinity wastewater by adsorption onto graphene oxide. J. Environ. Chem. Eng. 7, 103106. http://dx.doi.org/10.1016/j.jece.2019.103106.

Ewis, D., Benamor, A., Ba-Abbad, M.M., Nasser, M., El-Naas, M., Qiblawey, H., 2020. Removal of oil content from oil-water emulsions using iron oxide/bentonite nano adsorbents. J. Water Process Eng. 38, 101583. http://dx.doi.org/10.1016/j.jwpe.2020.101583.

Fahmi, Mochamad Zakki, Prasetya, Roch Adi, Dzikri, Muhammad Fathan, Sakti, Satya Candra Wibawa, Yuliarto, Brian, Irzaman, Ferdiansjah, 2020. Mater. Chem. Phys. 250, http://dx.doi.org/10.1016/j.matchemphys.2020.123055.

Ghoochian, M., Panahi, H.A., Sobhanardakani, S., Taghavi, L., Hassani, A.H., 2019. Synthesis and application of Fe_3O_4/SiO_2/thermosensitive/PAMAM-CS nanoparticles as a novel adsorbent for removal of tamoxifen from water samples. Microchem. J. 145, 1231–1240. http://dx.doi.org/10.1016/j.microc.2018.12.004.

Gurav, R., Bhatia, S.K., Choi, T.R., Choi, Y.K., Kim, H.J., Song, H.S., Park, S.L., Lee, H.S., Lee, S.M., Choi, K.Y., Yang, Y.H., 2021. Adsorptive removal of crude petroleum oil from water using floating pinewood biochar decorated with coconut oil-derived fatty acids. Sci. Total Environ. 781, 146636. http://dx.doi.org/10.1016/j.scitotenv.2021.146636.

Hambali, E., Sakti, S.C.W., Fahmi, M.Z., Wahyudianto, F.E., Nuryono Yessi, P., Yani, M., Sinurat, E., Pratama, B.S., 2018. Effect of extraction time and Na_2CO_3 concentration on the characteristics of alginate extracted from sargassum sp. IOP Conf. Ser. Earth Environ. Sci. 209, http://dx.doi.org/10.1088/1755-1315/209/1/012033.

Hoang, A.T., 2018. A report of the oil spill recovery and treatment technologies to reduce the marine environment pollution. Int. J. e-Navig. Marit. Econ. 9, 35–49.

Hoang, A.T., Bui, X.L., Pham, X.D., 2018a. A novel investigation of oil and heavy metal adsorption capacity from as-fabricated adsorbent based on agricultural by-product and porous polymer. Energy Sources A 40, 929–939. http://dx.doi.org/10.1080/15567036.2018.1466008.

Hoang, A.T., Le, V.V., Al-Tawaha, Abdel Rahman M. Said, Nguyen, D.N., Al-Tawaha, Abdel Razzaq M. Said, Noor, M.M., Pham, V.V., 2018b. An absorption capacity investigation of new absorbent based on polyurethane foams and rice straw for oil spill cleanup. Pet. Sci. Technol. 36, 361–370. http://dx.doi.org/10.1080/10916466.2018.1425722.

Hoang, A.T., Nguyen, X.P., Duong, X.Q., Huynh, T.T., 2021. Sorbent-based devices for the removal of spilled oil from water: a review. Environ. Sci. Pollut. Res. 28, 28876–28910. http://dx.doi.org/10.1007/s11356-021-13775-z.

Jamwal, R., Amit Kumari, S., Sharma, S., Kelly, S., Cannavan, A., Singh, D.K., 2021. Recent trends in the use of FTIR spectroscopy integrated with chemometrics for the detection of edible oil adulteration. Vib. Spectrosc. 113, http://dx.doi.org/10.1016/j.vibspec.2021.103222.

Ke, C.Y., Chen, L.Y., Qin, F.L., Sun, W.J., Wang, S.C., Zhang, Q.Z., Zhang, X.L., 2021. Biotreatment of oil sludge containing hydrocarbons by Proteus mirabilis SB. Environ. Technol. Innov. 23, 101654. http://dx.doi.org/10.1016/j.eti.2021.101654.

Leonardo, S., Prieto-Simón, B., Campàs, M., 2016. Past, present and future of diatoms in biosensing. TrAC - Trends Anal. Chem. 79, 276–285. http://dx.doi.org/10.1016/j.trac.2015.11.022.

Li, T., Song, F., Zhang, J., Liu, S., Xing, B., Bai, Y., 2020. Pyrolysis characteristics of soil humic substances using TG-FTIR-MS combined with kinetic models. Sci. Total Environ. 698, 134237. http://dx.doi.org/10.1016/j.scitotenv.2019.134237.

Lv, X., Zhang, Y., Fu, W., Cao, J., Zhang, J., Ma, H., Jiang, G., 2017. Zero-valent iron nanoparticles embedded into reduced graphene oxide-alginate beads for efficient chromium (VI) removal. J. Colloid Interface Sci. 506, 633–643. http://dx.doi.org/10.1016/j.jcis.2017.07.024.

Mahmoud, M.A., 2020. Oil spill cleanup by raw flax fiber: Modification effect, sorption isotherm, kinetics and thermodynamics. Arab. J. Chem. 13, 5553–5563. http://dx.doi.org/10.1016/j.arabjc.2020.02.014.

Mapelli, F., Scoma, A., Michoud, G., Aulenta, F., Boon, N., Borin, S., Kalogerakis, N., Daffonchio, D., 2017. Biotechnologies for marine oil spill cleanup: Indissoluble ties with microorganisms. Trends Biotechnol. 35, 860–870. http://dx.doi.org/10.1016/j.tibtech.2017.04.003.

Metin, A.Ü., Doğan, D., Can, M., 2020. Novel magnetic gel beads based on ionically crosslinked sodium alginate and polyanetholesulfonic acid: Synthesis and application for adsorption of cationic dyes. Mater. Chem. Phys. 256, http://dx.doi.org/10.1016/j.matchemphys.2020.123659.

Mota dos Santos, A.A., Cordeiro, G.C., 2021. Investigation of particle characteristics and enhancing the pozzolanic activity of diatomite by grinding. Mater. Chem. Phys. 270, http://dx.doi.org/10.1016/j.matchemphys.2021.124799.

Narita, Y., Sakti, S.C.W., Akemoto, Y., Tanaka, S., 2019. Ultra-rapid removal of cationic organic dyes by novel single- and double-stranded DNA immobilized on quaternary ammonium magnetic chitosan. J. Environ. Chem. Eng. 7, 103308. http://dx.doi.org/10.1016/j.jece.2019.103308.
Nasrollahzadeh, M., Sajjadi, M., Iravani, S., Varma, R.S., 2021. Starch, cellulose, pectin, gum, alginate, chitin and chitosan derived (nano)materials for sustainable water treatment: A review. Carbohydr. Polym. 251, 116986. http://dx.doi.org/10.1016/j.carbpol.2020.116986.
Neves, M.D.G., Poppi, R.J., 2020. Authentication and identification of adulterants in virgin coconut oil using ATR/FTIR in tandem with DD-SIMCA one class modeling. Talanta 219, http://dx.doi.org/10.1016/j.talanta.2020.121338.
Nizami, M.Z.I., Takashiba, S., Nishina, Y., 2020. Graphene oxide: A new direction in dentistry. Appl. Mater. Today 19, 100576. http://dx.doi.org/10.1016/j.apmt.2020.100576.
Nuryono, M., Kuncaka, A., Sakti, S.C.W., 2016. Functionalization of Fe_3O_4/SiO_2 with N-(2-aminoethyl)-3-aminopropyl for sorption of $[AuCl_4]^-$. Indones. J. Chem. 16, http://dx.doi.org/10.14499/ijc-v16i2p130-137.
Nuryono, N., Miswanda, D., Sakti, S.C.W., Rusdiarso, B., Krisbiantoro, P.A., Utami, N., Otomo, R., Kamiya, Y., 2020. Chitosan-functionalized natural magnetic particle@silica modified with (3-chloropropyl)trimethoxysilane as a highly stable magnetic adsorbent for gold(III) ion. Mater. Chem. Phys. 255, 123507. http://dx.doi.org/10.1016/j.matchemphys.2020.123507.
Nuryono, Mutia Rosiati, N., Rusdiarso, B., Sakti, S.C.W., Tanaka, S., 2014. Coating of magnetite with mercapto modified rice hull ash silica in a one-pot process. Springerplus 3, 515. http://dx.doi.org/10.1186/2193-1801-3-515.
Phogat, S., Saxena, A., Kapoor, N., Aggarwal, C., Tiwari, A., 2021. Diatom mediated smart drug delivery system. J. Drug Deliv. Sci. Technol. 63, 102433. http://dx.doi.org/10.1016/j.jddst.2021.102433.
Raj, K.G., Joy, P.A., 2015. Coconut shell based activated carbon–iron oxide magnetic nanocomposite for fast and efficient removal of oil spills. J. Environ. Chem. Eng. 3, 2068–2075. http://dx.doi.org/10.1016/j.jece.2015.04.028.
Rigueto, C.V.T., Rosseto, M., Nazari, M.T., Ostwald, B.E.P., Alessandretti, I., Manera, C., Piccin, J.S., Dettmer, A., 2021. Adsorption of diclofenac sodium by composite beads prepared from tannery wastes-derived gelatin and carbon nanotubes. J. Environ. Chem. Eng. 9, 105030. http://dx.doi.org/10.1016/j.jece.2021.105030.
Sakthi Sri, S.P., Taj, J., George, M., 2020. Facile synthesis of magnetite nanocubes using deep eutectic solvent: an insight to anticancer and photo-Fenton efficacy. Surf. Interfaces 20, 100609. http://dx.doi.org/10.1016/j.surfin.2020.100609.
Sakti, S.C.W., Laily, R.N., Aliyah, S., Indrasari, N., Fahmi, M.Z., Lee, H.V., Akemoto, Y., Tanaka, S., 2020. Re-collectable and recyclable epichlorohydrin-crosslinked humic acid with spinel cobalt ferrite core for simple magnetic removal of cationic triarylmethane dyes in polluted water. J. Environ. Chem. Eng. 8, 104004. http://dx.doi.org/10.1016/j.jece.2020.104004.
Sakti, S.C.W., Narita, Y., Sasaki, T., Nuryono Tanaka, S., 2015. A novel pyridinium functionalized magnetic chitosan with pH-independent and rapid adsorption kinetics for magnetic separation of Cr(VI). J. Environ. Chem. Eng. 3, 1953–1961. http://dx.doi.org/10.1016/j.jece.2015.05.004.
Sakti, S.C.W., Wijaya, R.A., Indrasari, N., Fahmi, M.Z., Widati, A.A., Abdulloh, Nuryono, Chen, C.H., 2021. Magnetic hollow buoyant alginate beads achieving rapid remediation of oil contamination on water. J. Environ. Chem. Eng. 9, 104935. http://dx.doi.org/10.1016/j.jece.2020.104935.
Shahrashoub, M., Bakhtiari, S., 2021. The efficiency of activated carbon/magnetite nanoparticles composites in copper removal: Industrial waste recovery, green synthesis, characterization, and adsorption–desorption studies. Microporous Mesoporous Mater. 311, 110692. http://dx.doi.org/10.1016/j.micromeso.2020.110692.
Singh, A.K., Ketan, K., Singh, J.K., 2017. Simple and green fabrication of recyclable magnetic highly hydrophobic sorbents derived from waste orange peels for removal of oil and organic solvents from water surface. J. Environ. Chem. Eng. 5, 5250–5259. http://dx.doi.org/10.1016/j.jece.2017.09.060.
Soares, S.F., Rodrigues, M.I., Trindade, T., Daniel-da-Silva, A.L., 2017. Chitosan-silica hybrid nanosorbents for oil removal from water. Colloids Surf. A 532, 305–313. http://dx.doi.org/10.1016/j.colsurfa.2017.04.076.
Song, X., Chai, Z., Zhu, Y., Li, C., Liang, X., 2019. Preparation and characterization of magnetic chitosan-modified diatomite for the removal of gallic acid and caffeic acid from sugar solution. Carbohydr. Polym. 219, 316–327. http://dx.doi.org/10.1016/j.carbpol.2019.04.043.
Song, X., Li, C., Chai, Z., Zhu, Y., Yang, Y., Chen, M., Ma, R., Liang, X., Wu, J., 2021. Application of diatomite for gallic acid removal from molasses wastewater. Sci. Total Environ. 765, 142711. http://dx.doi.org/10.1016/j.scitotenv.2020.142711.
Sriram, G., Kigga, M., Uthappa, U.T., Rego, R.M., Thendral, V., Kumeria, T., Jung, H.Y., Kurkuri, M.D., 2020. Naturally available diatomite and their surface modification for the removal of hazardous dye and metal ions: A review. Adv. Colloid Interface Sci. 282, 102198. http://dx.doi.org/10.1016/j.cis.2020.102198.
Tarhan, İ., 2020. A comparative study of ATR-FTIR, UV–visible and fluorescence spectroscopy combined with chemometrics for quantification of squalene in extra virgin olive oils. Spectrochim. Acta A 241, http://dx.doi.org/10.1016/j.saa.2020.118714.
Thyng, K.M., 2019. Deepwater Horizon Oil could have naturally reached Texas beaches. Mar. Pollut. Bull. 149, 110527. http://dx.doi.org/10.1016/j.marpolbul.2019.110527.
Wang, Y., Liu, X., Yu, X., Zheng, X., 2018. Assessing response capabilities for responding to ship-related oil spills in the Chinese Bohai Sea. Int. J. Disaster Risk Reduct. 28, 251–257. http://dx.doi.org/10.1016/j.ijdrr.2018.02.040.
Yaacob, S.F.F.S., Razak, N.S.A., Aun, T.T., Rozi, S.K.M., Jamil, A.K.M., Mohamad, S., 2018. Synthesis and characterizations of magnetic bio-material sporopollenin for the removal of oil from aqueous environment. Ind. Crops Prod. 124, 442–448. http://dx.doi.org/10.1016/j.indcrop.2018.08.024.
Yadav, M., Das, M., Savani, C., Thakore, S., Jadeja, R., 2019. Maleic anhydride cross-linked β-cyclodextrin-conjugated magnetic nanoadsorbent: An ecofriendly approach for simultaneous adsorption of hydrophilic and hydrophobic dyes. ACS Omega 4, 11993–12003. http://dx.doi.org/10.1021/acsomega.9b00881.
Yang, K., Ren, J., Cui, Y., Wang, Y., Shah, T., Zhang, Q., Zhang, B., 2021. Fabrication of porous tubular carbon fibers from the fruits of platanus orientalis and their high oil adsorption properties. J. Environ. Chem. Eng. 9, 105706. http://dx.doi.org/10.1016/j.jece.2021.105706.

Diatomaceous earth incorporated floating magnetic beads for oil

ORIGINALITY REPORT

13%	12%	6%	5%
SIMILARITY INDEX	INTERNET SOURCES	PUBLICATIONS	STUDENT PAPERS

MATCH ALL SOURCES (ONLY SELECTED SOURCE PRINTED)

3%

★ oar.icrisat.org

Internet Source

Exclude quotes	On	Exclude matches	< 5 words
Exclude bibliography	On		